Numerical Phase Front Propagation for the Laser Interferometer Space Antenna

Miltiadis V. Papalexandris[a], and Eugene Waluschka[b]

[a]Jet Propulsion Laboratory, California Institute of Technology, Pasadena, CA 91109.
[b]NASA Goddard Space Flight Center, Greenbelt, MD 20771.

ABSTRACT

The present article reports on numerical studies of phase front propagation for the Laser Interferometer Space Antenna (LISA). The main objective is to determine the sensitivity of the average phase of the metrology beam with respect to fluctuations of the pointing of the beam. For this purpose, the metrology beam is propagated numerically along the interferometric arm of the instrument. The effects of the obscurations from the secondary mirror and its supporting struts are studied in detail. Further, the effects of random wavefront distortions that occur due to imperfections of the optical elements are estimated through a series of Monte Carlo simulations. The results of this study can be used to determine design requirements for the instrument.

Keywords numerical beam propagation, tilt sensitivity, interferometry.

1. INTRODUCTION

The Laser Interferomenter Space Antenna (LISA) [1], [2], is a long-baseline, Michelson-type interferometer, currently under development, for the detection of gravitational waves. The instrument will consist of three sun-orbiting spacecraft distanced 5 million kilometers from each other, see Fig. 1. Inside each spacecraft there are two proof masses, carefully insulated so that they are subject to gravitational forces only, thus forming three very long arms with end points the flat front face of the proof masses. Detection of gravitational waves will be performed by precise measurements of the length variations of the three arms. These length variations are calculated by measuring the phase delays for laser beams that have traversed these arms. For this purpose, each spacecraft is equipped with two telescopes pointing at the other two spaceraft.

The present article reports on the results of detailed numerical computations of the phase of the optical beam propagated along the interferometric arm of LISA. The proposed methodology for numerical phase front propagation consists of three steps. The first step is the verification of the accuracy of the available algorithms. The second one is the numerical propagation of a truncated Gaussian beam over large distances. The third step is the computation of the average phase of the propagated field over the receiving aperture.

The primary objective of this study is the calculation of the sensitivity of the average phase of the metrology beam with respect to jitter or off-axis pointing of the beam. In particular, we are concerned with the estimation of the effects of obscurations and random wavefront distortion in the exit pupil. The results obtained from the numerical simulations can be employed to determine various design parameters for the instrument, such as pointing stability requirement, *etc.*

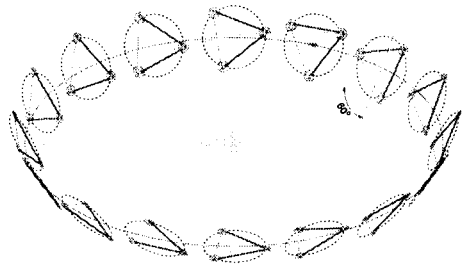

Figure 1. Schematic of the Laser Interferometer Space Antenna.

2. DESCRIPTION OF THE NUMERICAL METHOD

Consider an isotropic, homogeneous, non-dispersive and non-magnetic medium covering the half space $\Omega \equiv (x, y, z \geq 0)$. Further, consider an aperture, denoted by Γ, at the plane $z = 0$. The aperture is illuminated by a normally incident plane wave of wavelength λ. According to the paraxial approximation, the electromagnetic field $U(x, y, z)$ can be written as

$$U(x, y, z) \;=\; \exp(jkz) \times u(x, y, z)\;, \tag{1}$$

where $k = 2\pi/\lambda$, and $u(x, y, z)$ is slowly varying with respect to z. Then, the field satisfies the paraxial equation

$$\left(\frac{\partial^2}{\partial x^2} + \frac{\partial^2}{\partial y^2} + j2k\frac{\partial}{\partial z}\right) u(x, y, z) \;=\; 0\,, \qquad (x, y, z) \in \Omega\,. \tag{2}$$

The boundary condition at the plane of the emitting aperture is given by the Kirchoff approximation

$$U(x, y, 0) = \begin{cases} u(x, y, 0), & \text{if } (x, y) \in \Gamma \\ 0, & \text{otherwise}\,. \end{cases} \tag{3}$$

The boundary condition at infinity is given by the Sommerfeld radiation condition which states that at large distances the field should consist of simple waves propagating away from the emitting aperture.

Applying standard techniques, *i.e.*, Green's theorem, the following integral representation of the field can be obtained, [3],

$$U(x, y, z) \;=\; \frac{\exp(jkz)}{j\lambda z} \exp\left(\frac{jk}{2z}(x^2 + y^2)\right) \times$$
$$\iint_{-\infty}^{+\infty} u(\xi, \eta, 0)\; \exp\left(\frac{jk}{2z}(\xi^2 + \eta^2)\right)\; \exp\left(-\frac{j2\pi}{\lambda z}(x\xi + y\eta)\right)\; d\xi\, d\eta\,. \tag{4}$$

We observe that this representation is a Fourier-type integral and therefore, it can be evaluated numerically via a Discrete Fourier Transform (DFT). In the present study we employed the DFT that is based on the Goertzel-Reinsch algorithm, see Papalexandris & Redding [4]. This algorithm performs summation of finite trigonometric series by employing the Clenshaw's recurrence formulae that hold for trigonometric functions, Stoer & Bulirsch [5]. This method provides speed and accuracy and works well in equispaced grids. The summation of the series is performed in a way that prevents round-off errors from growing, thus ensuring stability of the computations. Another advantage of this method is the freedom in the choice of the sampling intervals at the (x, y) plane where the field is computed. It is worth mentioning that application of Fast Fourier Transforms (FFTs) for the numerical evaluation of the above integral is not advantageous because these algorithms do not allow scaling of the grid at the plane of the receiving aperture; see also the discussion in [4].

An alternative way to solve the paraxial equation (2) is the angular spectrum method, [2], which results in a different but completely equivalent Fourier-integral representation of the field. The final expression for the field is

$$U(x,y,z) \;=\; \exp(jkz) \iint_{-\infty}^{+\infty} \mathcal{F}\left(U\left(x,y,0\right)\right) \exp[-j\pi\lambda z(f_x^2 + f_y^2)] \times \exp[j2\pi(f_x x + f_y y)]\, df_x\, df_y\,, \tag{5}$$

where $\mathcal{F}(\cdot)$ denotes the Fourier transform of a fucntion.

This integral representation is also a Fourier integral. We observe, however, that the Fourier kernel becomes highly oscillatory as the propagation distance z increases. Therefore, this method can not give accurate results for large values of z unless the numerical resolution is increased significantly. Typically, the required resolution far exceeds current computational resources. For this reason, the angular spectrum method has not been employed in the present study.

The quantity of interest is φ, the average phase of the beam over the area of the receiving aperture, denoted by A. It is defined as the phase of the integral of the field, $I(z)$, over A,

$$\varphi \;\equiv\; \tan^{-1}\left(\frac{Im(I)}{Re(I)}\right)\,, \tag{6}$$

where

$$I(z) \;\equiv\; \int_A U(x,y,z)\, dx\, dy\,. \tag{7}$$

The average phase φ is evaluated directly from (6). The integral of the optical I is computed via the two-dimensional extension of Simpson's rule, once the field $U(x, y, z)$ has been evaluated numerically with the algorithm outlined above. More involved quadrature algorithms, such as Gauss integration, have not been employed because they require non-equispaced abscissas. Furthermore, grid-convergence studies have shown that Simpson's rule provides accuracy at the order of $10^{-6}\lambda$, [4].

3. NUMERICAL RESULTS

In this section we present results for the numerically propagated phase front. In particular, we are interested in the sensitivity to tilt of the average phase of the beam. By the term "sensitivity" we mean the difference between average phase when the emitting aperture is tilted and the average phase when the aperture has the nominal no-tilt position. In general, sensitivity values above $10^{-5}\lambda$ are not considered acceptable.

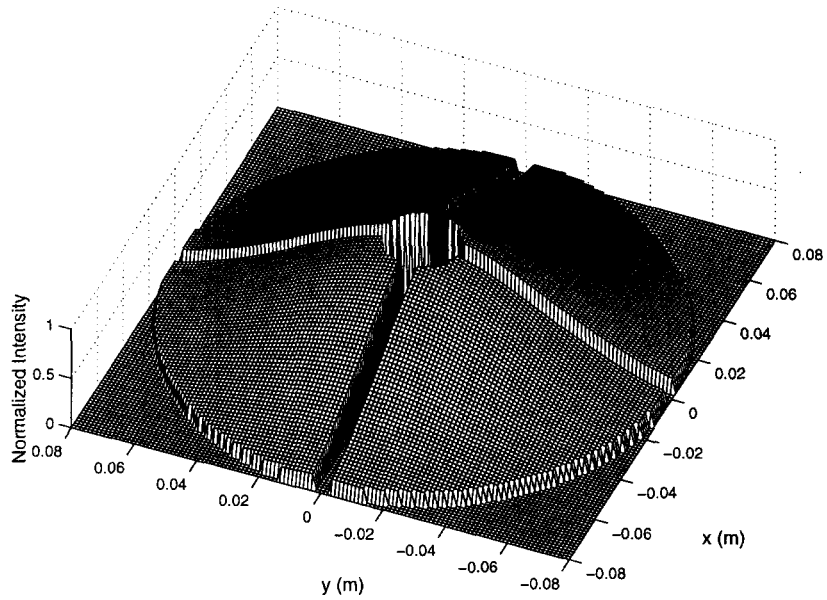

Figure 2. Intensity plot of the emitted wavefront subject to obscurations from the secondary mirror and its supporting struts.

There are two main sources of aberrations for the emitted wavefront. These are distortions due to optical imperfections and obscurations from the secondary mirror and its 4 supporting struts. The distorions on the optical beam are random, in the sense that their functional form can not be known precisely. However, it is assumed that statistical information about them is available. Such distortions are due to various imperfections that occur during the fabrication and assembly phase, such as surface figure errors, inhomogeneity of the refractive index, polarization effects on the beam splitters, and others.

In the numerical tests conducted, both the emitting and the receiving apertures are circular with diameter $d = 30\ cm$. In the current design of LISA, the emitting aperture is the primary mirror of one of the two telescopes of a spacecraft. It also coincides with the exit pupil of the optical system. The receiving aperture is the primary mirror of a telescope of another spacecraft. The emitting and receiving apertures are at a distance $z = 5 \times 10^9\ m$ from each other and their centers lie on the optical axis.

The optical beam is Gaussian with waist $w_0 = 8\ cm$ at the emitting aperture [6], *i.e.*,

$$U(x,y,0) = \begin{cases} \exp\left(-\left(x^2+y^2\right)/w_0^2\right), & \text{if } \sqrt{x^2+y^2} \leq d/2\,, \\ 0, & \text{otherwise}. \end{cases} \tag{8}$$

The wavelength is $\lambda = 1.064\ \mu m$. Therefore, the acceptable level of sensitivity is, approximately, $10^{-5}\lambda \simeq 10\,pm$. It is worth mentioning that the beam's diameter at the plane of the receiving aperture is more than $42\ km$, while the peak intensity of the electromagnetic field has been reduced by 5 orders of magnitude.

As a first step, we studied the effect of the obscuring elements in the absense of random distortions. Plot of the normalized intensity of the field at the emitting aperture is shown in Fig. 2. The aperture is first tilted at an angle θ with respect to the $x-$ axis. Subsequently the average phase at the receiving aperture is computing numerically with the procedure outlined in the previous section and compared with the corresponding value at the nominal (no tilt) position.

The numerical results clearly show that the sensitivity of the average phase is very small (less than $1\,pm$ at tilt angle $\theta = 3\,\mu rads$, see Fig. 3. It is important to mention that negligible sensitivity was also observed

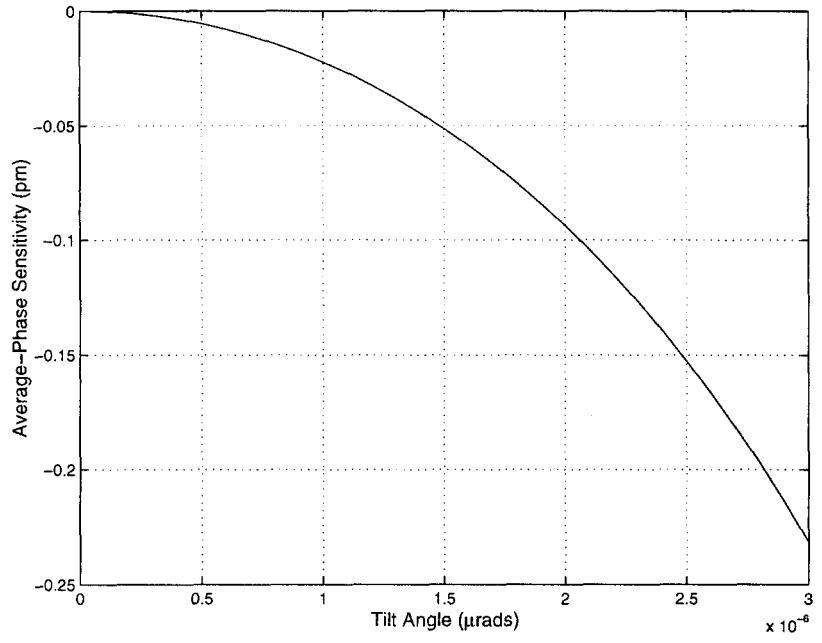

Figure 3. Average phase sensitivity to tilt for an obscured emitted wavefront.

when the aperture was unobscured. The reason for such small average-phase sensitivity is that in both cases (obscured and unobscured) the field at the emitting aperture remains symmetric with respect to the $x-$ and $y-$ axes. In the case of obscured emitting aperture, this symmetry results in cancellations of the diffraction effects due to the supporting struts. When the secondary mirror was considered to be supported by 3 struts instead of 4, a dramatic increase in the average-phase sensitivity to tilt was observed due to loss of symmetry. In particular, the sensitivity at $\theta = 3\,\mu rads$ was $1442\,pm$.

Next, the effects of the addition of random distortions were studied. These distortions have the form $\exp(jkg(x,y))$. The aberration function $g(x,y)$ can be discontinuous across the apertureand its spectral content might extend to considerably high frequencies. Therefore, the aberration function can not be efficiently modeled by Zernicke polynomials. The spectrum of $g(x,y)$ is assumed to obey a (known) Power Spectral Density (PSD) law. In general, $g(x,y)$ is given by

$$g(x,y) \;=\; a\,\frac{f(x,y)-\bar{f}}{\sigma_f}\,, \tag{9}$$

where $f(x,y)$ is the "normalized aberration function", $\bar{f}$ and σ_f are the mean value and standard deviation of f respectively, and a is the amplitude parameter. The normalized aberration function $f(x,y)$ is given as a convolution over the emitting aperture,

$$f(x,y) \;=\; \int_{\Gamma} \nu(\xi,\eta)\,h(x-\xi,y-\eta)\,d\xi\,d\eta\,, \tag{10}$$

with $\nu(\xi,\eta)$ being a random matrix of zero mean and variance equal to 1, and $h(\xi,\eta)$ being the PSD function.

It is further assumed that the Fourier transform of the PSD function, $\mathcal{F}(h)$, obeys a power law. In other

words,

$$\mathcal{F}(h) = \left(\frac{1}{1 + \left(\sqrt{f_x^2 + f_y^2}/\alpha \right)^{\beta}} \right)^{1/2}, \tag{11}$$

where (f_x, f_y) is the spatial frequency pair, α is the (dimensionless) half-power point, and β is the exponent of the power law. The values of α and β can be estimated from previously fabricated mirrors. In the present study, we set $\alpha = 0.15$ and $\beta = 3$. It should be mentioned that the PSD function does not have to be monotonic; in principle, any function whose Fourier transform exists could be used. In the present study, the choice of PSD function and its parameters was based on data fitting with images from the Hubble Space Telescope.

Using a random number generator, values of $\nu(x, y)$ can be taken at discrete points inside the emitting aperture. By virtue of the convolution theorem, the Fourier transform of $f(x, y)$ is written as $\mathcal{F}(f) = \mathcal{F}(\nu)\ \mathcal{F}(h)$, with $\mathcal{F}(h)$ given by (11). Applying a discrete inverse Fourier transform on $\mathcal{F}(f)$, we can obtain values of $f(x, y)$ at discrete locations inside the emitting aperture. Then, we can directly generate realizations of wavefront aberrations $g(x, y)$ by employing relation (9). Such a representative realization is plotted in Fig. 4a. Results for the average-phase sensitivity to tilt for different realization of $g(x, y)$ are shown in Fig. 4b. It can be observed that the effect of such aberrations can be quite large, up to 12 nm for $\theta = 3\ \mu rads$ tilt angle.

Fig. 4 also shows that the sensitivity to tilt can vary widely from one realization to another. Therefore, the derivation of design requirements must rely upon statistical analysis of the effects of such wavefront distortions. The proposed methodology consists of the following steps.

i) We select values of rms distortion, that is values of the amplitude parameter a. The range of rms values is chosen so that it covers the rms values that we expect to have given the current fabrication capabilities and cost estimates for the optical system. For each rms value, a set of 1000 Monte Carlo simulations is conducted to produce curves of phase sensitivity to tilt.

More specifically, for each rms value, realizations of $\nu(\xi, \eta)$ are produced with a random number generator. For each realization the corresponding wavefront distortion is calculated via (9) (11). This distortion is added to the wavefront of the emitting aperture and the electromagnetic field is calculated for various tilt angles, up to $\theta = 3\ \mu rads$. Then, we can plot the curve of the average phase sensitivity to tilt under this particular random distortion, similar to the curves plotted in Fig. 4. This procedure is repeated for 1000 random wavefront realizations for each rms value a.

ii) The maximum acceptable average-phase error for tilt around the y-axis is set at 10 pm. Then the tilt angle that yields this maximum acceptable error is computed for each phase sensitivity curve that was produced from the Monte Carlo simulations. This way we can generate, for each rms value a, a distribution of tilt angles that yield this error. Histogram of the distribution for $a = \lambda/20$ is plotted in Fig. 5a. Normalizing the bin counts of each histogram yields discrete values of the corresponding probability density function, $\rho(\theta; a)$ of the tilt-angle distribution.

iii) The mean value $\bar{\theta}$ and the standard deviation σ_θ of each distribution are evaluated via numerical quadrature with Simpson's rule.

The functional dependence of the mean $\bar{\theta}$ on a is plotted in Fig. 6. The curves $\bar{\theta} \pm \sigma_\theta$ are also plotted. These two curves define a "band" of expected tilt angles that yield a 10 pm average-phase error for a given

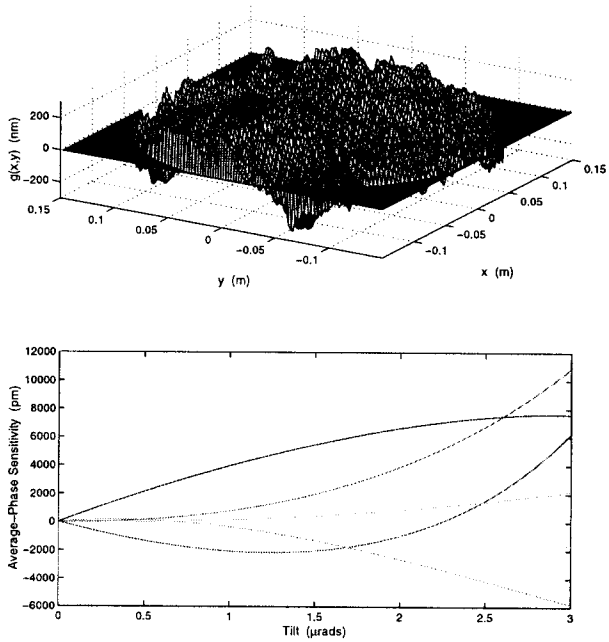

Figure 4. **a**: Plot of a realization of a random wavefront distortion.**b**: Average phase sensitivity to tilt for different realizations of $g(x, y)$.

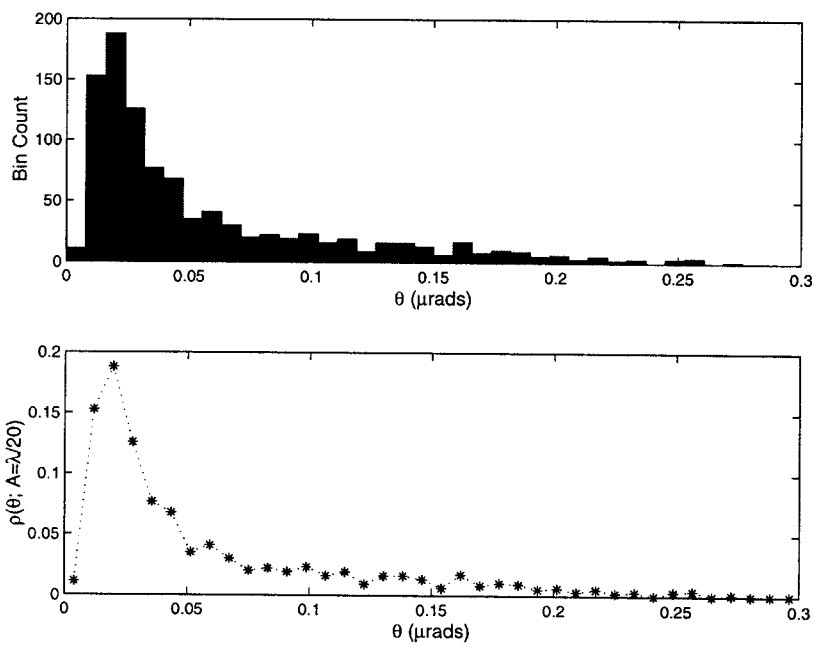

Figure 5. **a)** Monte-Carlo simulations: histogram of tilt angles that produce 10 pm average-phase error. rms value of wave-front distortion, $a = \lambda/20$. **b)** Probability density function resulting from normalization of the values of the above histogram.

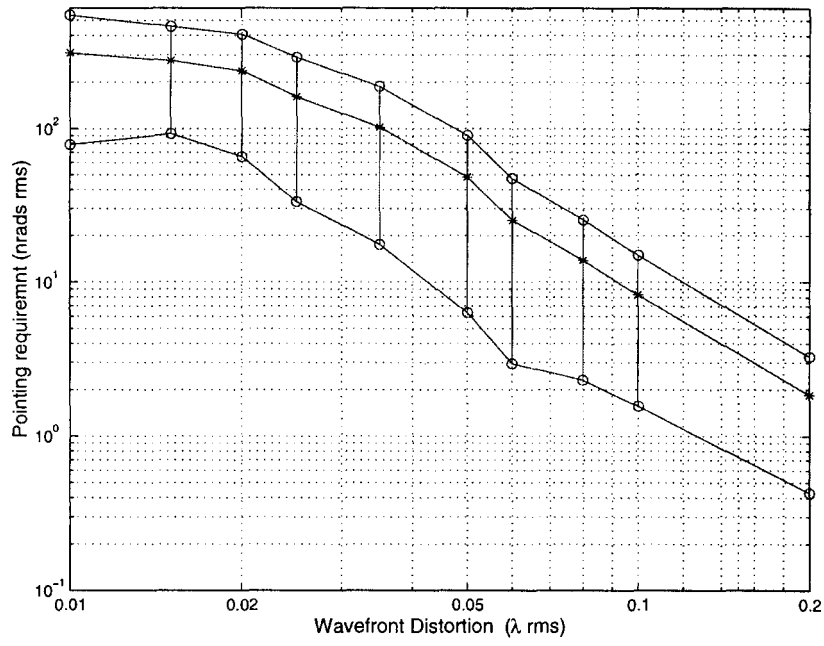

Figure 6. Pointing requirement as a function of rms value of wavefront distorion. The band shown in the plot is defined by the curves $\bar{\theta} - \sigma_\theta$ and $\bar{\theta} - \sigma_\theta$.

rms value of the wavefront distortion a. The lower boundary of this band, *i.e.*, the points on the curve $\bar{\theta} - \sigma_\theta$, define the pointing requirement of the emitting aperture for a particular wavefront distortion. For example, if assuming that the fabrication of the optical elements will be such that the distortion will have an rms value $a = 25\% \, \lambda$, then the pointing requirement is 70 *nrads*. The plot of Fig. 6 indicates that for large a the pointing requirement grows almost logarithmically. As a gets small, however, the lower bound remains almost constant at 70 *nrads*.

4. CONCLUSIONS

In this paper, a procedure for numerical propagation of the metrology beam of a Large-Baseline Space Interferometer was presented. The proposed procedure relies on highly accurate physical optics algorithms and a probabilistic approach for modeling of wavefront distortions due to optical imperfections. Numerical tests showed that this procedure is accurate and robust. Therefore, it can be employed as a reliable simulation tool for the study of the optical performance of the system and the derivation of various design requirements such as pointing stability, defocus, and other effects.

A detailed study of pointing stability of the metrology beam was also conducted. First, the effects of obscurations on the average phase were computed. It was observed that the obscurations can increase the sensitivity to tilt dramatically if they destroy the symmetry of the field even when the amount of energy lost to obscurations is small. On the contrary, when the obscurations are symmetric, their effect is minimal even when they absorb a lot of energy from the electromagnetic field. Subsequently, the effects of random wavefront distortions were studied. It was observed that these effects are in general more important than those arising from aperture obscurations. For rms distortion values $a > 2\% \, \lambda$, the pointing requirement grows almost logarithmically, but at smaller values of a it becomes almost constant.

ACKNOWLEDGMENTS

This work was prepared by the Jet Propulsion Laboratory, California Institute of Technology, under a contract with the National Aeronautics and Space Administration. The authors gratefully acknowledge Dr. A. Abramovici of JPL for his suggestions and support.

REFERENCES

[] Folkner, W.M., Bender, P.L., and Stebbins, R.T., *Laser Interferometer Space Antenna: Mission Concept Study*, JPL Publication 97-16, 1998.

[] Walushka, E., "LISA far-field phase patterns", *SPIE Proceedings*, Vol. **3779**, 1999.

[] Goodman, J.W., *Introduction to Fourier Optics*, McGraw-Hill, New York, NY, 1996.

[] Papalexandris, M.V., and Redding, D.C., "Calculation of Diffraction Effects on the Average Phase of an Optical Field," *J. Opt. Soc. Am., A*, Vol. **17**, pp. 1763-1772, 2000.

[] Stoer, J., and Bulirsch, R., *Introduction to Numerical Analysis*, Springer Verlag, New York, NY, 1980.

[] Siegman, A.E., *Lasers*, University Science Books, Mill Valley, California, 1977.